NASA TN D-73

TECHNICAL NOTE

D-73

COMPARISON OF CALCULATED AND MEASURED STALL BOUNDARIES OF A HELICOPTER ROTOR AT ADVANCE RATIOS FROM 0.3 TO 0.4

By John L. McCloud III and George B. McCullough

Ames Research Center
Moffett Field, Calif.

NATIONAL AERONAUTICS AND SPACE ADMINISTRATION

WASHINGTON September 1959

NATIONAL AERONAUTICS AND SPACE ADMINISTRATION

TECHNICAL NOTE D-73

COMPARISON OF CALCULATED AND MEASURED STALL BOUNDARIES OF A HELICOPTER ROTOR AT ADVANCE RATIOS FROM 0.3 TO 0.4

By John L. McCloud III and George B. McCullough

SUMMARY

Computations were made of the performance characteristics of a helicopter rotor by the method of NACA TN 3747. The computed characteristics are compared with the measured characteristics of a geometrically similar rotor reported in NACA TN 4367. The calculated and measured stall boundaries based on rotor torque indications were roughly parallel, but the calculated boundary represented rotor lift coefficients which were lower than the experimental values.

In operational regions free of calculated blade stall, the agreement between calculated and measured values of rotor thrust or lift was good. The computed propulsive force was greater than the measured force; whereas the opposite was true of the torque. The absence of hub drag and windage terms in the calculations could account for part of these discrepancies.

INTRODUCTION

The potential top speed of helicopters is limited by stalling of the retreating rotor blades; in this operational region for rotors with moderate blade twist the stall begins at the blade tip and spreads inboard as forward speed is increased. The attendant vibration imposes the practical upper limit to forward speed. A full-scale study of retreating blade stall as affected by a change in blade section profile is reported in reference 1. Comparisons of the experimentally measured stall boundaries with those predicted by simplified rotor theories or by empirical formulae were poor. The advent of high-speed, electronic digital computing machines, however, makes it practical to apply more refined rotor theory to the prediction of retreating blade stall and thus to avoid many of the simplifying assumptions of the elementary theory. It would be of obvious benefit if it could be shown that these more refined theories gave good predictions of the stall boundary and thus enable the investigation of a wide range of blade sections without recourse to the time-consuming and

costly experimental approach. The study reported herein was undertaken to determine to what degree the theory of reference 2 could be used for this purpose.

It was planned initially to examine the accuracy with which the calculations predicted the stall boundary for each of the two blade section profiles used for the study reported in reference 1. In addition, it was also planned to determine the accuracy with which the shift in stall boundary with change in airfoil section was predicted. Although airfoil section data applicable through a 360° angle-of-attack range existed for only one of the two blade sections, it was assumed that linearized, approximate post-stall characteristics could be used for either section, or for any section. Preliminary calculations showed this assumption to be erroneous. Reasonably accurate rotor characteristics could be calculated only if realistic airfoil data were used throughout the complete angle-of-attack range. It should be possible to improve the accuracy of the calculations by taking into account the effects on section characteristics of Reynolds number and Mach number as they vary around the rotor disk. Since the experimental results of reference 1 showed no effect of tip speed within the range of tip speeds employed, and since the effect of Reynolds number on the section characteristics of the "practical construction" blades is uncertain, the inclusion of these refinements in the calculations was not considered warranted. The study was restricted, therefore, to comparisons of rotor characteristics for the rotor having the NACA 0012 airfoil sections for which adequate section data existed (ref. 3).

This report presents the results of the study with particular emphasis placed on the prediction of retreating blade stall.

NOTATION

Positive directions of forces and moments are shown in the following sketches.

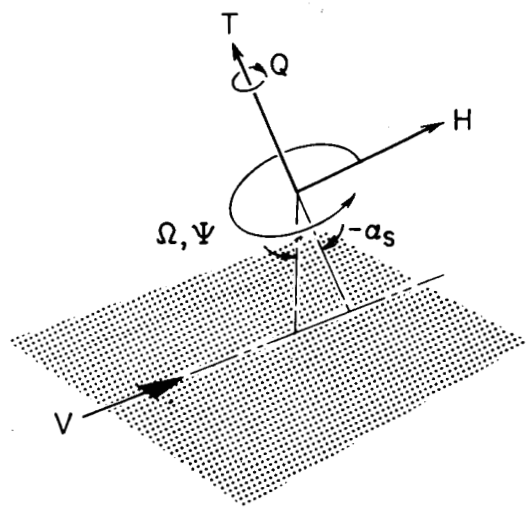

SHAFT AXES

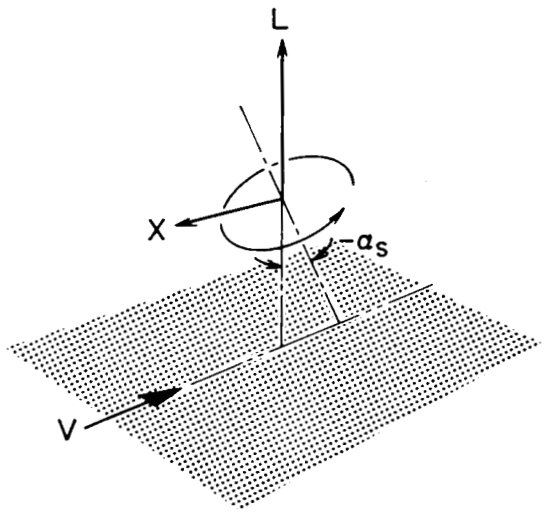

TUNNEL AXES

a_o, a_1, b_1 coefficients in Fourier series,
$\beta = a_o - a_1 \cos \psi - b_1 \sin \psi \ . \ . \ .$, deg

c_{d_o} section drag coefficient

C_H in-plane drag coefficient, $\dfrac{H}{\rho(\Omega R)^2 \pi R^2}$

C_L lift coefficient, $\dfrac{L}{q\pi R^2}$

C_{L_R} rotor lift coefficient, $\dfrac{L}{\rho(\Omega R)^2 \pi R^2}$

c_l section lift coefficient

C_Q torque coefficient, $\dfrac{Q}{\rho(\Omega R)^2 \pi R^3}$

C_T thrust coefficient, $\frac{T}{\rho(\Omega R)^2 \pi R^2}$

C_X longitudinal force coefficient, $\frac{X}{q\pi R^2}$

H in-plane drag force perpendicular to shaft axis, lb

L lift force, lb

q dynamic pressure, $\frac{1}{2}\rho V^2$, lb/sq ft

Q shaft torque, lb-ft

R rotor radius, ft

T thrust force, parallel with shaft axis, lb

V airspeed, ft/sec

$\frac{V}{\Omega R}$ advance ratio

$\left(\frac{V}{\Omega R}\right)_{av}$ average value of advance ratio for a series of shaft angles

v induced inflow velocity at rotor, ft/sec

X longitudinal force, lb

α_r angle of attack of blade section, deg

α_s shaft angle (equivalent to control axis inclination), deg

β flapping angle (positive up), deg

$\theta_{0.75}$ blade section pitch angle, angle between line of zero lift of blade section and plane perpendicular to shaft axis measured at the 0.75 radius station, deg

λ inflow ratio, $\frac{V \sin \alpha_s - v}{\Omega R}$

μ tip-speed ratio, $\frac{V \cos \alpha_s}{\Omega R}$

ρ mass density of air, slugs/cu ft

ψ blade azimuth angle measured from downwind position in direction of rotation, deg

Ω rotor rotational speed, radians/sec

COMPUTATIONAL PROCEDURE

Physical Characteristics of Rotor

The physical characteristics of the hypothetical rotor used in the calculations were intended to be a reasonably good approximation to those of the real rotor of reference 1. Some minor differences exist such as a 1° larger blade twist, and differences in blade weight and mass distribution. It is believed, however, that these differences did not have any significant effects on the computed rotor characteristics because the difference in twist is small, and because large variations in mass characteristics have only a small effect on computed rotor characteristics (ref. 4). A listing of the physical characteristics of the hypothetical rotor and the real rotor is given in table I.

The airfoil section characteristics (c_l and c_{d_o} vs. α) assumed for the blade sections are those for the NACA 0012 taken from reference 3. These characteristics were inserted into the calculations in tabular form for every 2° angle of attack from 0° to 360°. Linear interpolation was used for intermediate angles. A plot of these blade section characteristics is shown in figure 1.

Method of Calculation

In order to parallel the wind-tunnel testing technique employed in the investigation reported in reference 1, cyclic pitch was not used. The independent variable used in the computations was inflow ratio λ. Computations were made for constant values of blade-angle setting, $\theta_{0.75}$, and tip-speed ratio, μ. The actual calculations were carried out by an electronic digital computing machine (otherwise the method of calculation would be extremely laborious) and were divided into the two parts of reference 2 and a third part as follows.

Part I calculations.- This is an iterative process which establishes the equilibrium position of the rotor blade about the flapping hinge, and hence the flapping motion. The flapping motion is expressed in terms of the Fourier coefficients, a_o, a_1, b_1, etc., for the first three harmonics which can be combined to give the flapping angle β. The iterations were terminated when the coefficients were within 0.005 radian of the previous value. From the flapping motion, local values of the velocity, section angle of attack, section lift coefficient, and section drag coefficient are calculated. For the present work, 180 points within the rotor disk were employed (10 radial stations at 18 azimuth positions).

Part II calculations.- The local blade section values computed in part I are integrated by Simpson's rule and converted into rotor force and torque coefficients about the shaft axis.

Part III calculations.- The shaft angle α_s is computed from the relationship

$$\tan \alpha_s = \frac{\lambda}{\mu} + \frac{C_T}{2\mu(\mu^2+\lambda^2)^{1/2}}$$

The shaft-axis force coefficients are converted into wind-axis coefficients, and the advance ratio $V/\Omega R$ is computed.

Range of Computations

Computations were made for two blade-angle settings at the three-quarter radius station ($\theta_{0.75} = 12^\circ$ and 15°), and for three values of tip-speed ratio ($\mu = 0.30$, 0.35, and 0.40). For each blade-angle setting and tip-speed ratio a sufficient range of inflow ratios was covered to result in a range of rotor thrust coefficients C_T from near 0 to a maximum of about 0.007; this includes the range in which retreating blade stall would be expected to be encountered.

Method of Comparing Wind-Tunnel and Computed Data

Since inflow ratio λ was the independent variable for each series of computations, the computed coefficients represent an operational condition for which both shaft angle α_s and advance ratio $V/\Omega R$ are varying in a fixed relationship. In order to make the computed data directly comparable with the wind-tunnel data (which were obtained at

substantially constant values of advance ratio $V/\Omega R$ with shaft angle α_s as the variable) the computed data were converted into the same form. To do this, the computed data (C_{L_R}, C_{x_R}, and C_Q) were first plotted as functions of α_s. These data were then replotted as functions of advance ratio $V/\Omega R$ for various integral values of α_s for the three series of computations representing values of tip-speed ratio μ of 0.30, 0.35, and 0.40. Curves were drawn through the three points corresponding to each value of shaft angle (actually the curves were nearly straight). These plots (one for each blade angle) were then cross-plotted at the same values of advance ratio as those used in the experiment. In this manner the computed rotor characteristics were converted into the same form as the experimental data.

RESULTS AND DISCUSSION

Computed Rotor Characteristics

Part I solutions.- In figure 2 is shown the progression of the stalled area as the inflow ratio becomes less negative. These plots were obtained by spotting on maps of the rotor disk the points at which the local section angle of attack exceeded the two-dimensional, steady-state section angle of attack for maximum lift of 14°. It can be noted that the stalled area starts later and spreads more rapidly as inflow ratio becomes less negative for the blade-angle setting of 12° than for 15°. In general, the stalled area covers the same portion of the rotor disk as has been indicated by tuft studies of real rotors in this operational region.

In figure 3 is shown the variation of the flapping coefficients, a_o, a_1, and b_1, as inflow ratio becomes less negative. The tick marks on the curves indicate the inflow ratios corresponding to the first appearance of a local section angle of attack of 14°, and are considered to represent the initial appearance of retreating blade stall. The curves are nearly linear for inflow ratios up to the tick marks then start to diverge. This does not mean, however, that the flapping motion becomes unstable. In figure 4(a) is shown the calculated flapping motion for one revolution of the rotor with the blade angle set for 12° and for three values of inflow ratio, one just below the initial appearance of stall, and two with increasing amounts of blade stall present. It can be seen that although the flapping motion is increasing as inflow ratio becomes less negative, there is no sudden increase with the initial appearance of blade stall. The experimentally measured flapping motion from reference 1 and reproduced in figure 4(b) to the same scale as the computed curves showed a similar progressive increase in flapping motion without discontinuity in the operational region where blade stall was encountered.

Part II solutions.- In figures 5 and 6 are presented the computed variations of thrust coefficient, in-plane drag coefficient, and torque coefficient with inflow ratio. (Also shown is the variation of $V/\Omega R$ with inflow ratio obtained from the part III solutions.) In general, the variations of the thrust and in-plane drag coefficients are relatively linear and increase as inflow ratio becomes less negative until after the initial appearance of blade stall as indicated by tick marks on the curves. The torque coefficient increases at first then tends to round over until after the initial appearance of blade stall when there is an upturn or increase of torque. Examination of the calculated torque due to lift and profile torque showed that the increase of torque was due to the rapid increase of blade profile drag which accompanied the spreading area of retreating blade stall.

Part III solutions and comparison with experiment.- The computed and experimental variations of rotor lift coefficient C_{L_R} with shaft angle are shown in figure 7 for three values of $V/\Omega R$. (The rotor lift coefficient C_{L_R} is based on tip speed instead of forward velocity.) It can be seen that the computed curves agree well with the experimental points up to the shaft angle at which the computed curves bend over. It was shown previously (figs. 5 and 6) that the departure from linearity of the force curves followed the initial appearance of blade stall as indicated by the occurrence of local blade angles of attack which exceeded the section angle of attack for maximum lift. (It should be mentioned that in the wind tunnel, the first indications of the effects of retreating blade stall were given by an increase in the measured torque and by changes in the blade pitching moment as discussed in reference 1. These first indications do not necessarily coincide with the initial appearance of retreating blade stall. The measured thrust coefficient and rotor lift coefficient curves, however, showed little tendency to bend over with increasing shaft angle, even for test runs that penetrated several degrees into the region of retreating blade stall. It should also be mentioned that tunnel wall constraint corrections were not applied to the experimental data because of uncertainty as to their validity, and because they would have little effect on the location of the stall boundary.) It is evident, then, that the computations as carried out herein predict rotor lift characteristics accurately only for operational conditions up to the calculated inception of retreating blade stall.

In figure 8 the computed and experimental variations of the longitudinal force coefficient with shaft angle are compared. The computed values are greater than the experimental values except for the higher shaft angles where the computed values tend to decrease more rapidly than the measured values. The more rapid decrease of the longitudinal force coefficient curves is probably associated with the same phenomenon that caused the computed lift curves to bend over with the inception of blade stall, whereas the measured curves continued relatively straight. It would be expected that the computed values of longitudinal force coefficient would be greater than the measured values because of the lack of the inclusion of a hub drag in the computations.

The computed and experimental variations of torque coefficient with shaft angle are shown in figure 9. In all cases the computed torque is less than the measured torque for the entire range of shaft angles. This difference would also be expected because of the lack of a hub "windage" torque in the computations. However, there is also a blade-angle effect because the difference is greater for the 15° blade angle than for the 12° blade angle. The upturns of the computed torque curves do not coincide with the initial appearance of blade stall as evidenced by the droop of the rotor lift coefficient curves, but occur at a less negative shaft angle. Apparently the decrease in induced power and in propulsive power offsets the increase of profile power for a small range of shaft angles following the inception of blade stall. However, neither the above mentioned discrepancy in the magnitude of the longitudinal force nor the discrepancy in the torque has any significant effect on the determination of the stall boundary.

Comparison of stall boundaries.- The experimentally determined stall boundary from reference 1 is compared in figure 10 with the stall boundary deduced from the computations. In both cases the "upturn" of the torque curves as shown in figures 5(b) and 6(b) was used as the stall indicator. Also shown are two curves which correspond to the initial appearance of stall (the tick marks of previous figures) for blade-angle settings of 12° and 15°. The computed stall boundary is approximately parallel with the experimental boundary, but is as much as 0.0006 rotor lift coefficient or 10 percent below it. Similar to the experimental result, no effect of blade-angle setting on the stall boundary was shown for the 12° and 15° blade settings used in the computations. One reason for this lack of blade-angle effect is due to the rapid build-up of the stalled area with the 12° blade-angle setting (fig. 2). Although the initial stall occurred sooner (i.e., at lower lift) for the 15° blade setting, the rate of increase of the stalled area was relatively slow. Thus, the early inception of stall is offset by the slow increase of stalled area so that the effect of blade stall on rotor torque makes itself felt at about the same value of rotor lift coefficient for both blade-angle settings.

The reasons that the computations predict a lower stall boundary than was measured experimentally are not clear, but since the difference must be connected with the maximum lift and stalling angle actually attained by the blade sections of the real rotor, or in other words with the input data inserted in the calculations, several possible reasons suggest themselves. One reason is the lack of inclusion of any three-dimensional effect in the input data such as would be caused by radial flow along the blade similar to the spanwise flow on swept wings. This would result in the attainment of higher section maximum lift coefficients and angles of attack for maximum lift than the corresponding two-dimensional values (ref. 5). A second reason is that since the stall is a local phenomenon, variations in inflow velocity may affect the inception and growth of the stalled area. The third reason is concerned with the effect of the oscillating flow on the maximum lift and stalling angle of the blade

sections. There are data (e.g., ref. 6) which tend to show that the time-averaged maximum lift and angle of attack for maximum lift are greater in oscillating flow than in steady flow. Another possible cause for the failure of the computed rotor characteristics to agree with the measured characteristics is the lack of inclusion of aeroelastic effects in the input data. It would seem obvious that there must be an appreciable effect of aeroelasticity in such a long, slender structure as a helicopter rotor blade. Any or all of the foregoing effects in combination could cause the use of steady-state two-dimensional airfoil data to predict the occurrence of blade stall too soon.

In the present calculations neither Reynolds number nor compressibility effects were taken into account. Where suitable data are available, these effects should be considered, especially for rotors designed to operate at high tip speeds where compressibility effects become important. No effect of tip speed was shown in the investigation reported in reference 1, however, the maximum rotational tip speed was 596 feet per second.

Calculations of rotor performance characteristics are hampered not only by lack of information on possible three-dimensional and oscillating flow effects, but also by the meagerness of suitable airfoil section data for a wide range of angles of attack. However, in the present case, the computations gave a more definite stall boundary than the chart solution of reference 4 which depends on the section angle of attack assumed for maximum lift. The stall boundary predicted by the computations also gave better agreement with the wind-tunnel measurements than various empirical formulae based on average blade loading such as the one given in reference 7.

CONCLUDING REMARKS

Computations were made of the performance characteristics of a helicopter rotor by means of high-speed, electronic digital computing machines and airfoil section data for section angles from 0° to 360°; these computations are compared with the measured characteristics of a similar full-scale rotor. It was found that:

1. The calculated and measured stall boundaries, based on rotor torque indications, were roughly parallel with each other, but the calculated boundary was lower.

2. In operational regions free of calculated blade stall, the agreement between the calculated and measured values of rotor thrust or lift was good.

3. The calculated values of propulsive force were greater than the measured values, and the calculated values of rotor torque were less than

the measured values. Both of these differences can be explained, in part at least, by the absence of rotor hub drag and windage terms in the calculations.

4. On the basis of this one comparison the method used to predict the stall boundary is reasonably accurate and merits further investigation as a means of assessing proposed changes of blade section for increasing helicopter forward speed.

Ames Research Center
National Aeronautics and Space Administration
Moffett Field, Calif., June 2, 1959

REFERENCES

1. McCloud, John L., III, and McCullough, George B.: Wind-Tunnel Tests of a Full-Scale Helicopter Rotor With Symmetrical and With Cambered Blade Sections at Advance Ratios From 0.3 to 0.4. NACA TN 4367, 1958.

2. Gessow, Alfred: Equations and Procedures for Numerically Calculating the Aerodynamic Characteristics of Lifting Rotors. NACA TN 3747, 1956.

3. Critzos, Chris C., Heyson, Harry H., and Boswinkle, Robert W., Jr.: Aerodynamic Characteristics of NACA 0012 Airfoil Section at Angles of Attack From 0° to 180°. NACA TN 3361, 1955.

4. Gessow, Alfred, and Tapscott, Robert J.: Charts for Estimating Performance of High-Performance Helicopters. NACA Rep. 1266, 1956. (Supersedes NACA TN's 3323 and 3482)

5. Hunton, Lynn W.: Effects of Finite Span on the Section Characteristics of Two 45° Sweptback Wings of Aspect Ratio 6. NACA TN 3008, 1953. (Supersedes NACA RM A52A10)

6. Halfman, Robert L., Johnson, H. C., and Haley, S. M.: Evaluation of High-Angle-of-Attack Aerodynamic-Derivative Data and Stall-Flutter Prediction Techniques. NACA TN 2533, 1951.

7. Stepniewski, W. Z.: Introduction to Helicopter Aerodynamics. Rev. ed., Rotary Aircraft Series No. 3, Rotorcraft Publishing Committee, Morton, Pa., 1955.

TABLE I.- PHYSICAL CHARACTERISTICS, IN PARAMETRIC FORM, USED IN COMPUTATIONS AND OF EXPERIMENTAL ROTOR

	Hypothetical rotor	Experimental rotor
Solidity	0.0651	0.065
Twist, deg	-8	-7
Radius of cutout, fraction of blade radius	0.259	0.259
Offset of flapping hinge, fraction of blade radius	0.0173	0.0174
Tip loss factor B	0.97	- - -
Blade mass parameters		
$\frac{\rho c R^4}{I_h}$	1.639	[1]1.37
$\frac{M_w}{I_h \Omega^2}$	0.00334	[1]0.0034
$\frac{e\Omega^2}{g}$	8.68	8.74
Blade weight (from attached point outboard), lb	- - -	150
Radial station of center of gravity of blade	- - -	116

where

c blade chord, ft

e offset of flapping hinge, ft

g acceleration of gravity, ft/sec^2

I_h mass moment of inertia of blade about flapping hinge, slug ft^2

M_w weight moment of blade about flapping hinge, lb-ft

[1]Based on experimentally measured values of I_h, M_w, and for Ω corresponding to a tip speed of 596 feet per second.

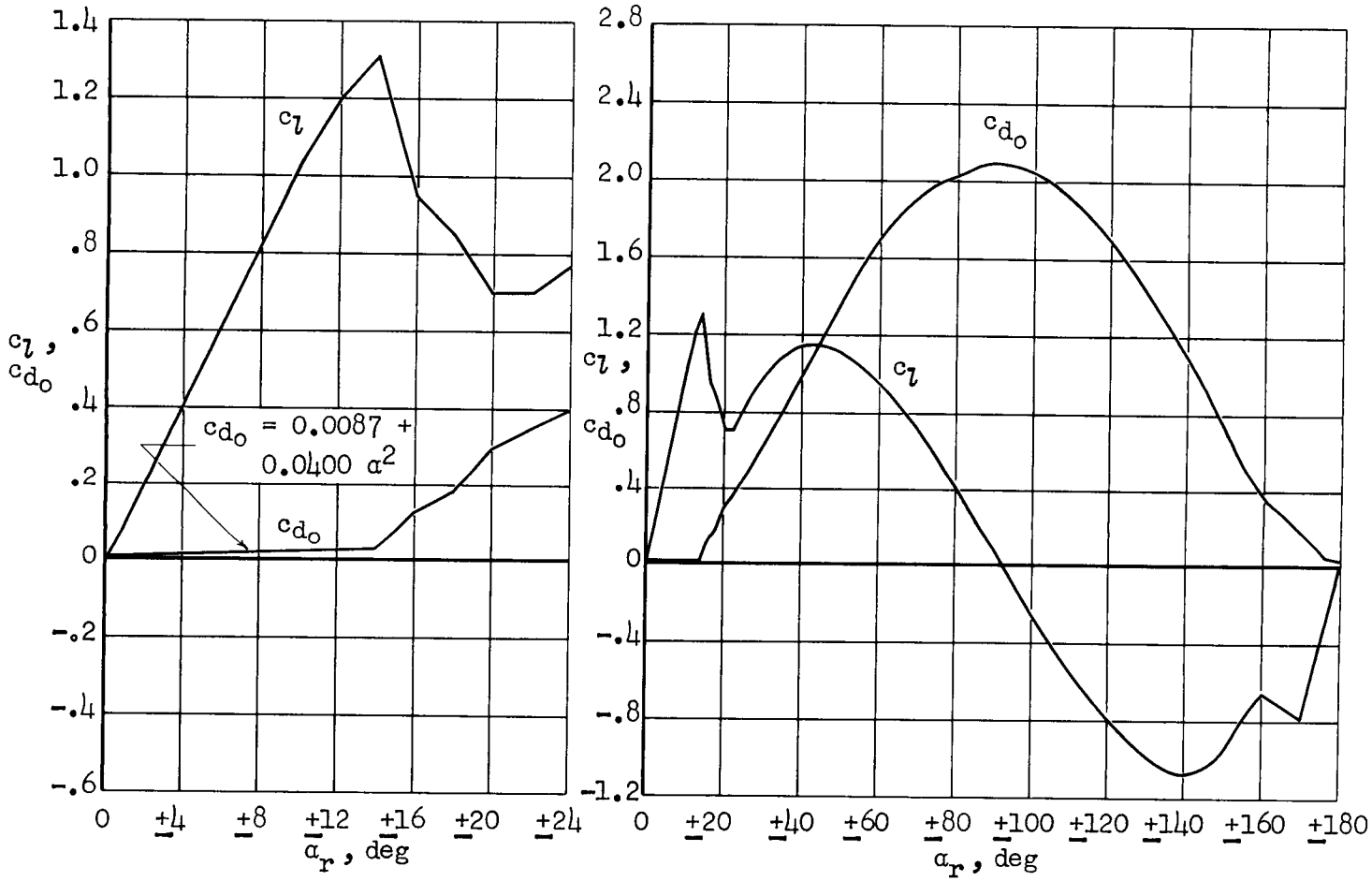

(a) 0° to ±24°

(b) 0° to ±180°

Figure 1.- Plots of airfoil section data used in calculations.

(a) $\theta_{0.75} = 12^{\circ}$

Figure 2.- Areas of computed retreating blade stall.

(b) $\theta_{0.75} = 15^{\circ}$

Figure 2.- Concluded.

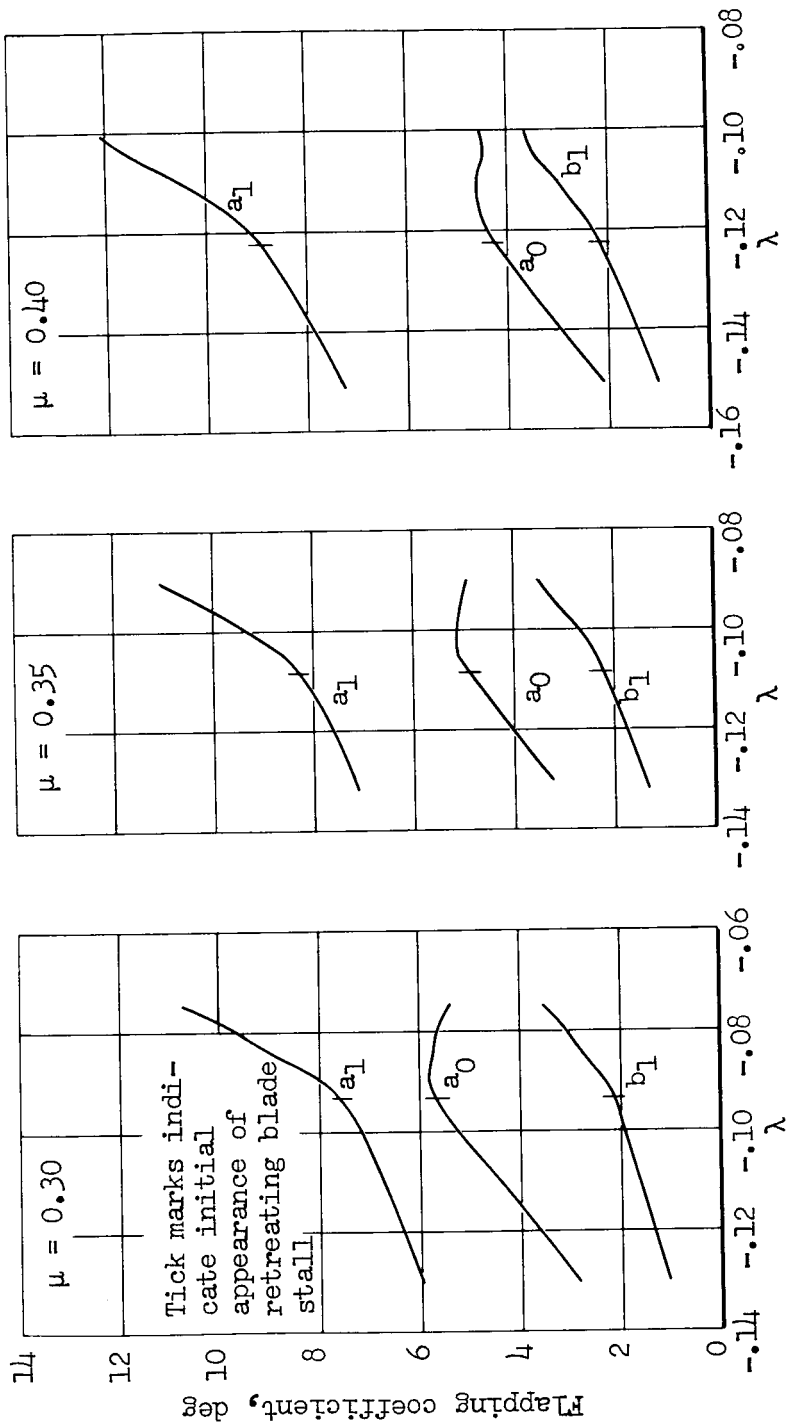

Figure 3.- Variation of flapping coefficients with λ; $\theta_{0.75} = 12^{\circ}$.

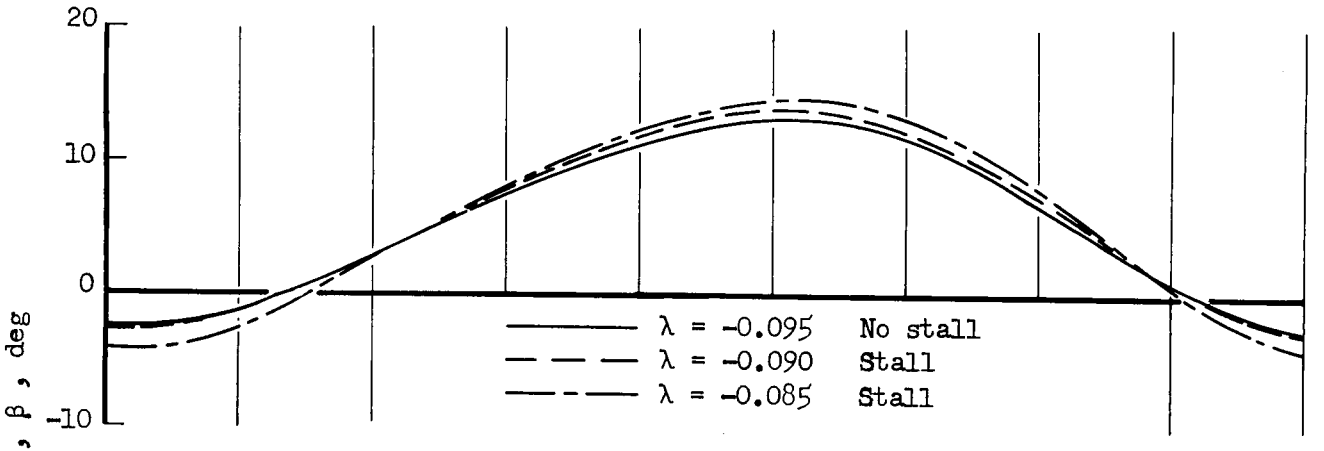

(a) Calculated flapping motion including third harmonic; $\theta_{0.75} = 12^{\circ}$, $\mu = 0.30$.

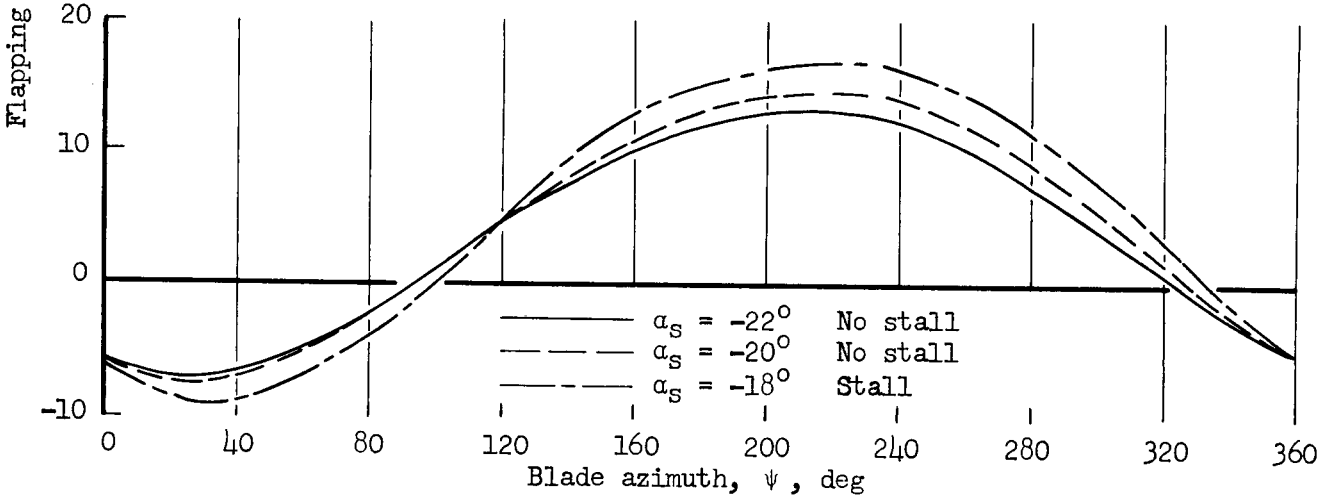

(b) Experimental flapping motion from reference 1; $\theta_{0.75} = 14^{\circ}$, $\mu = 0.36$.

Figure 4.- Calculated and experimental blade flapping motion.

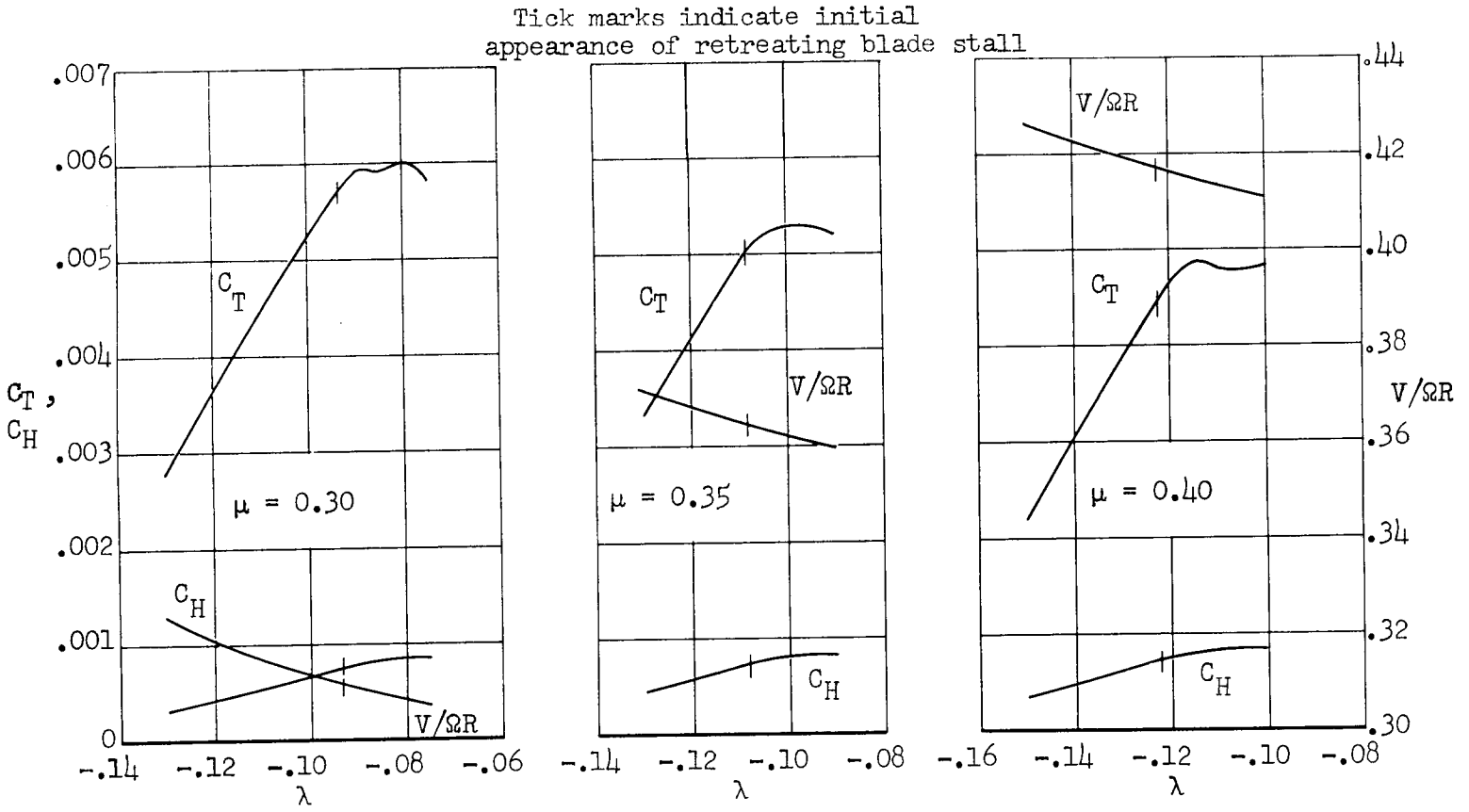

(a) C_T, C_H, $\frac{V}{\Omega R}$

Figure 5.- Computed thrust in-plane force, and torque coefficients; $\theta_{0.75} = 12^\circ$.

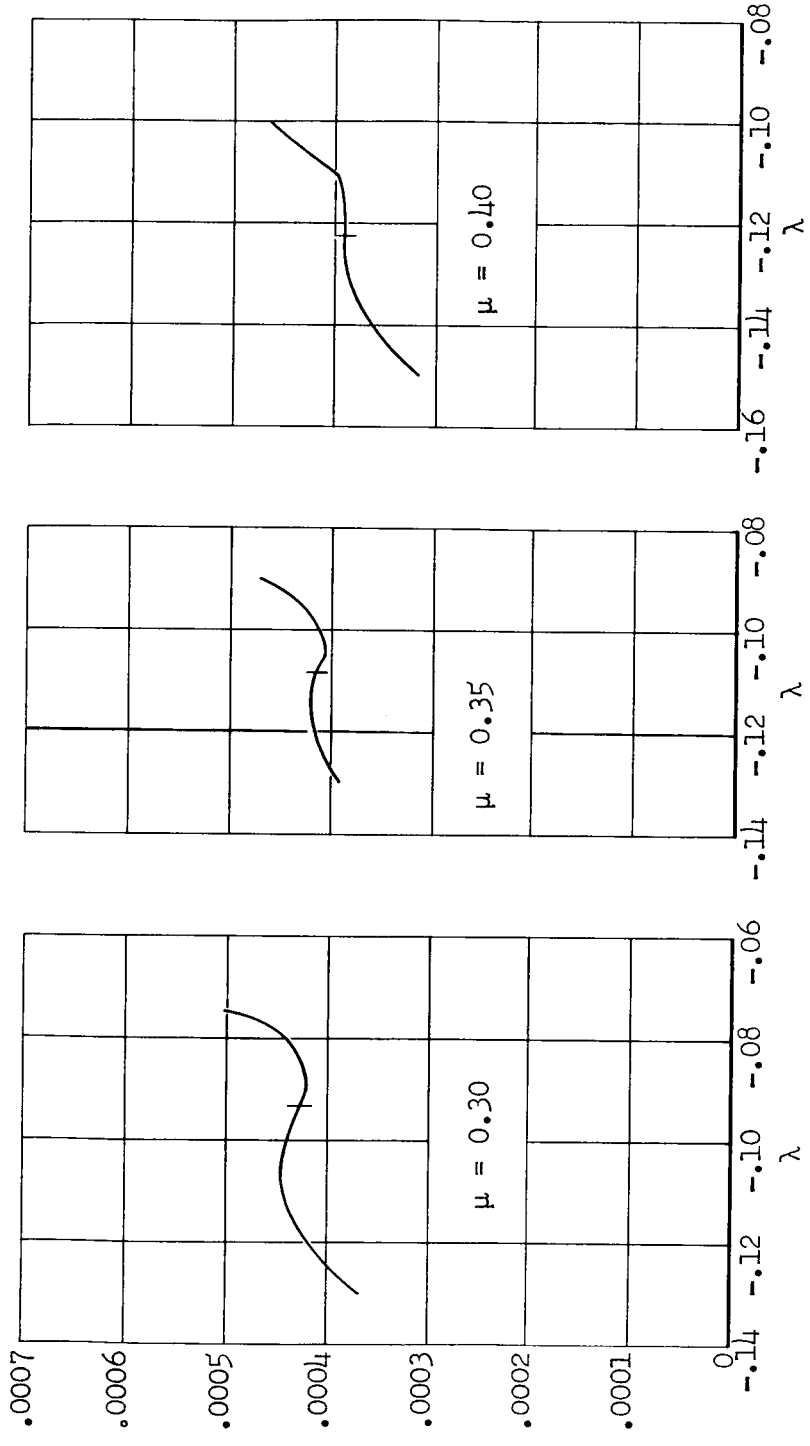

(b) C_Q

Figure 5.- Concluded.

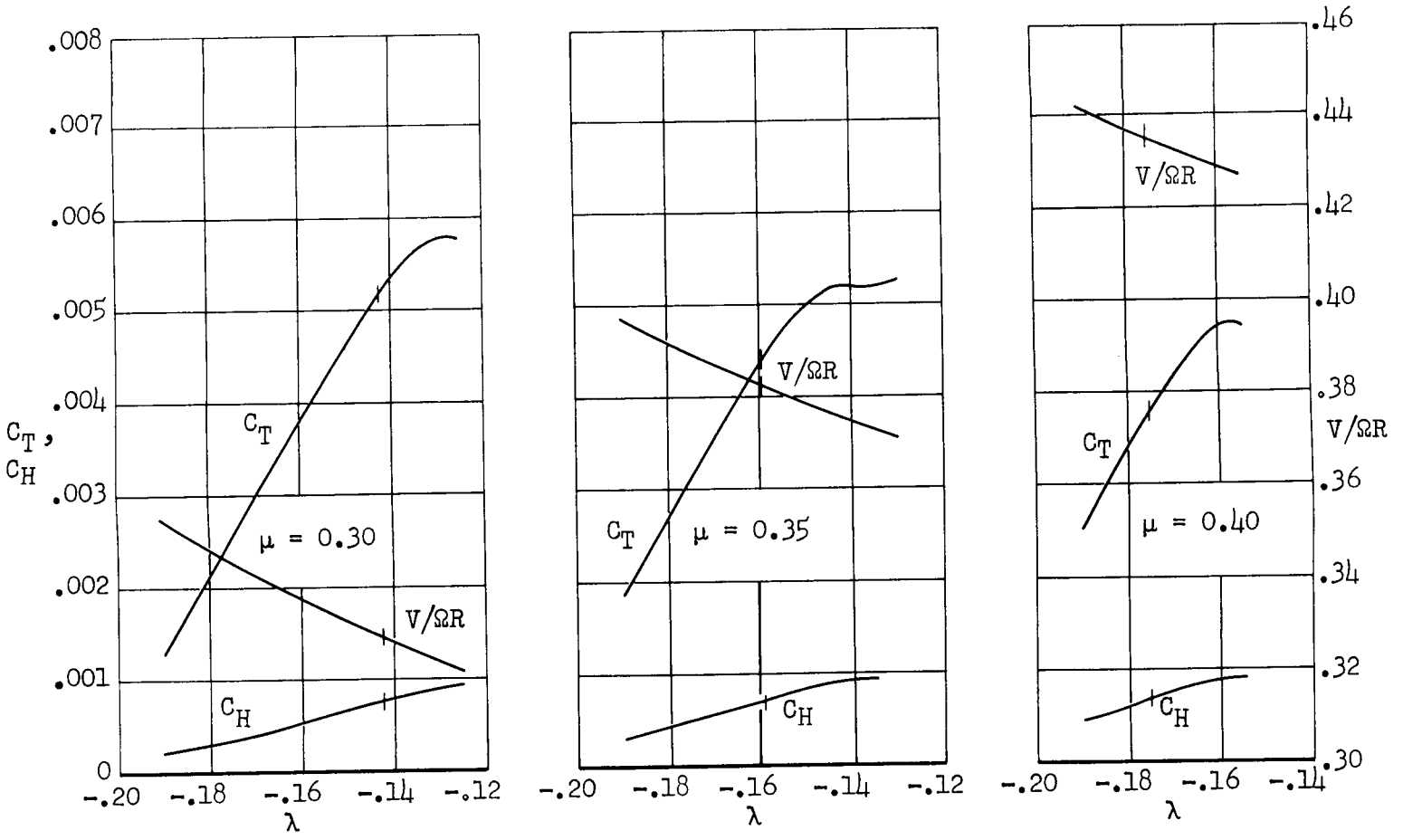

(a) C_T, C_H, $\frac{V}{\Omega R}$

Figure 6.- Computed thrust, in-plane force, and torque coefficients; $\theta_{0.75} = 15^\circ$.

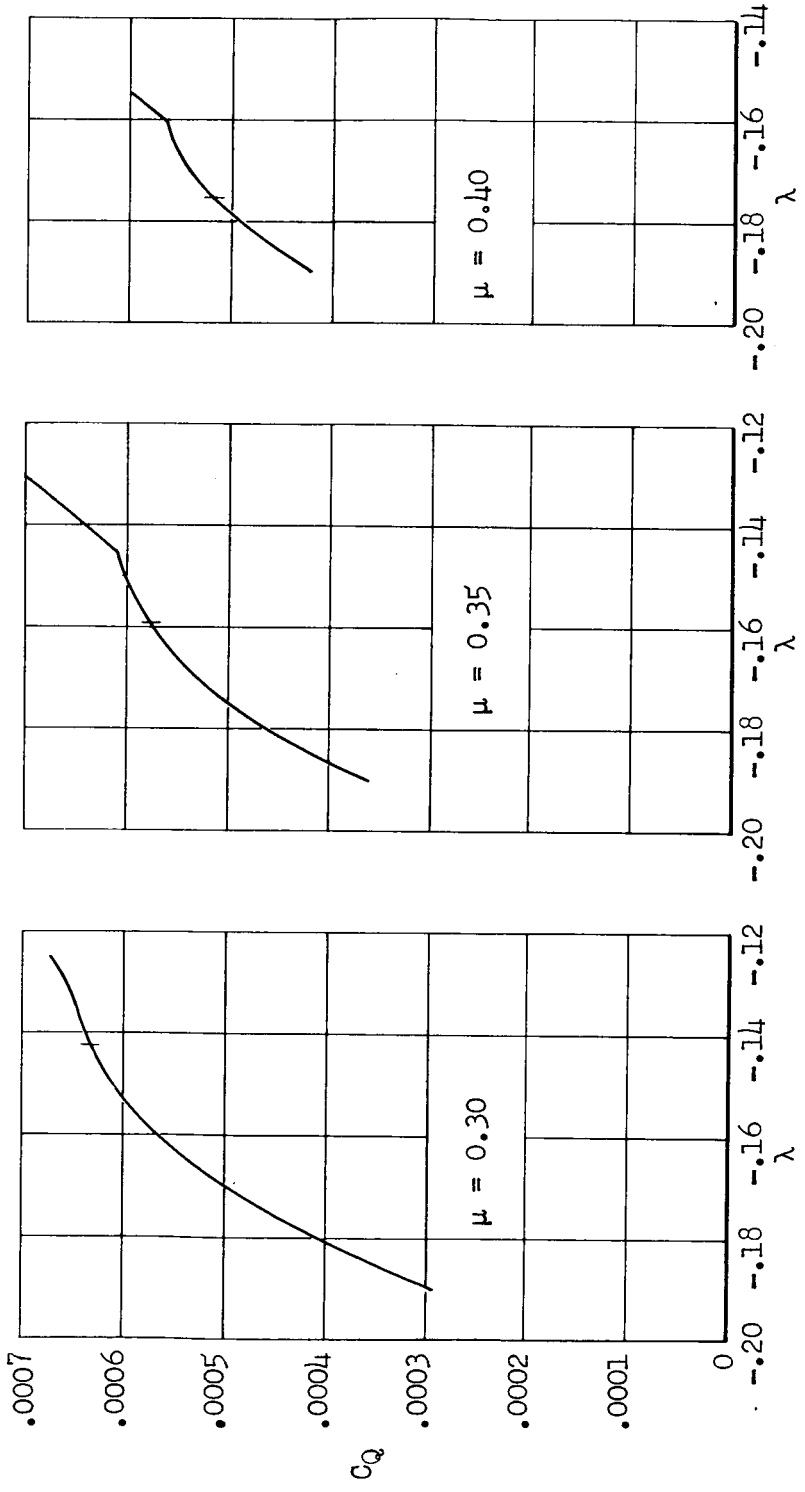

(b) C_Q

Figure 6.- Concluded.

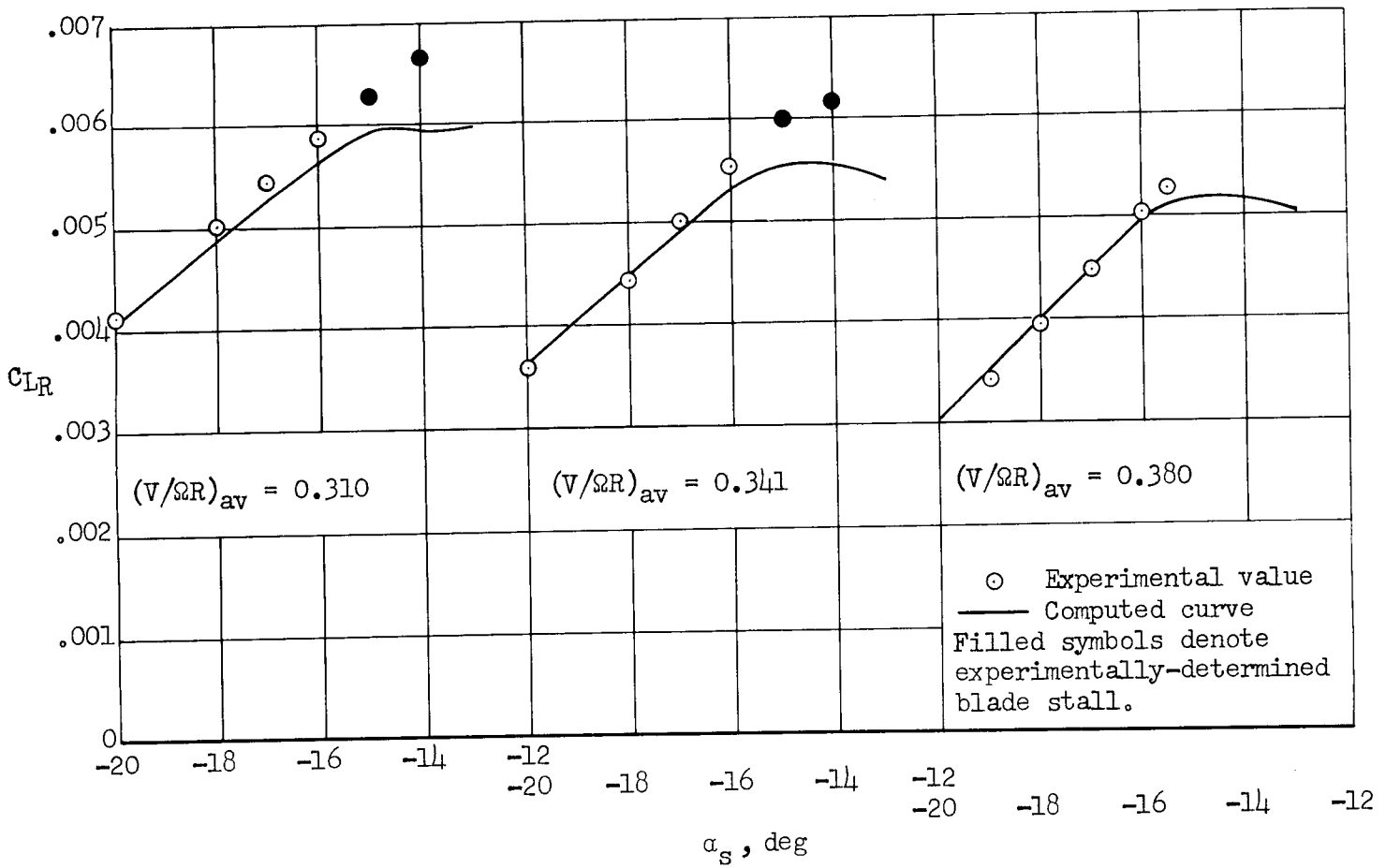

(a) $\theta_{0.75} = 12^\circ$

Figure 7.- Comparison of computed and experimental variations of C_{L_R} with shaft angle.

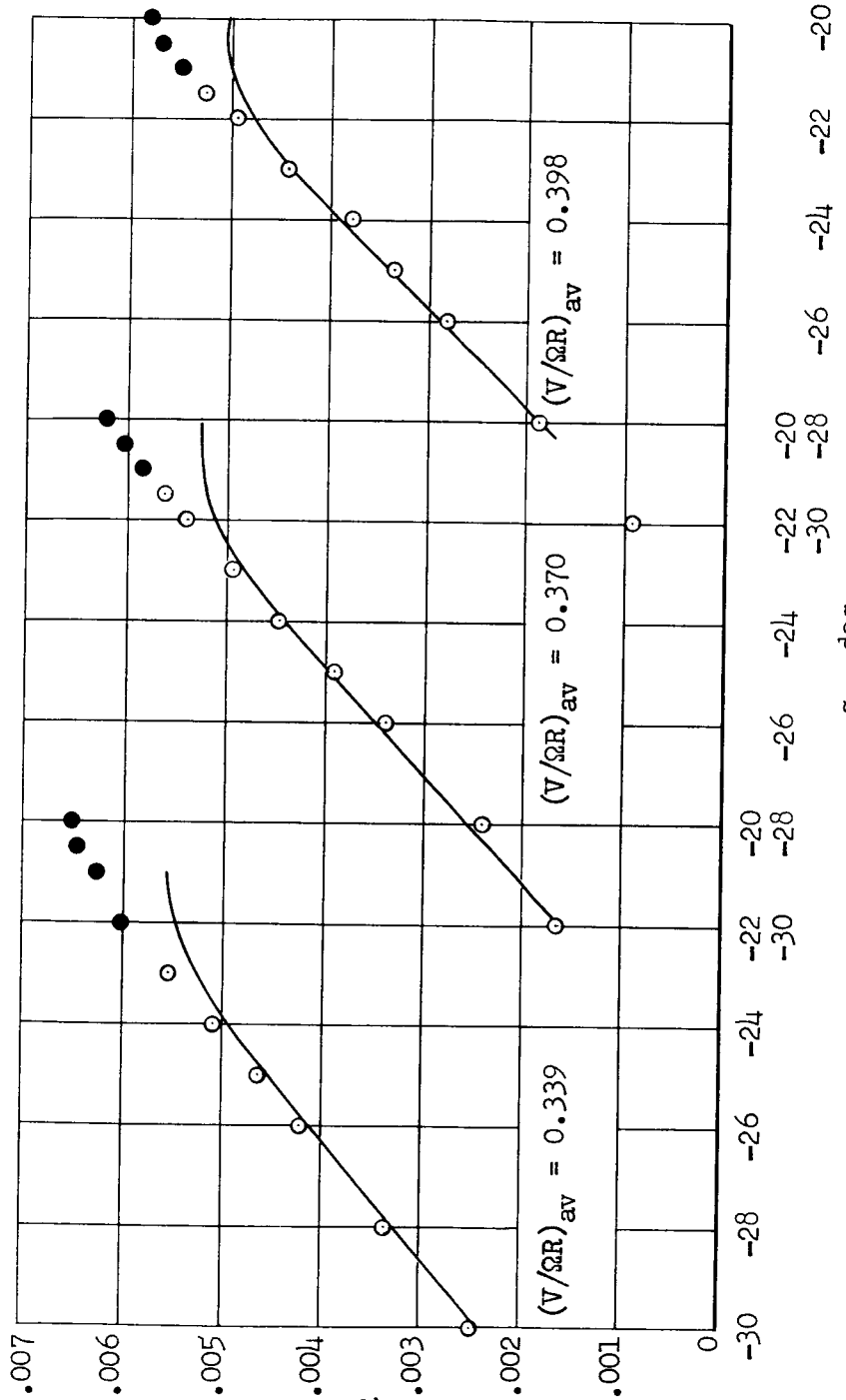

(b) $\theta_{0.75} = 15^{\circ}$

Figure 7.- Concluded.

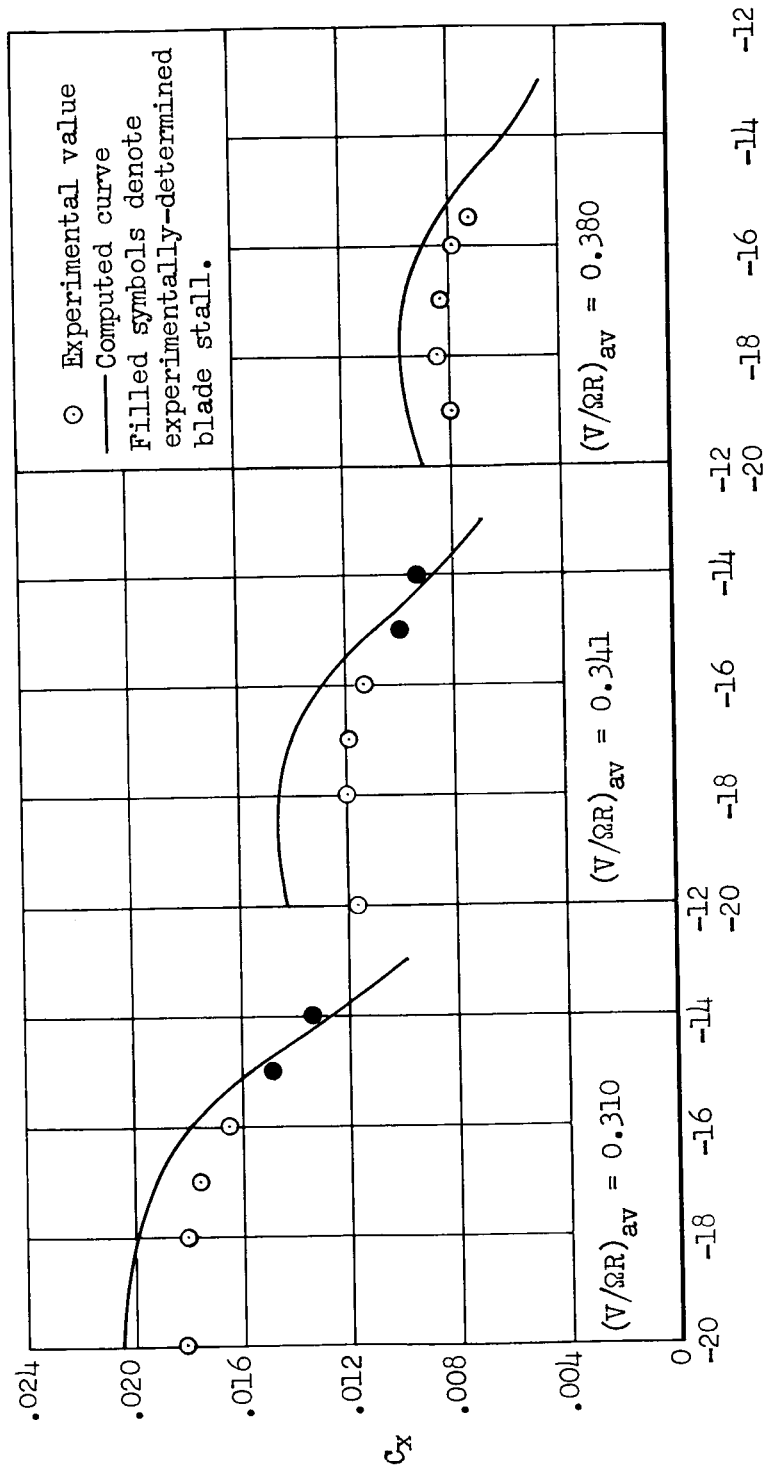

(a) $\theta_{0.75} = 12^\circ$

Figure 8.- Comparison of computed and experimental variations of C_x with α_s.

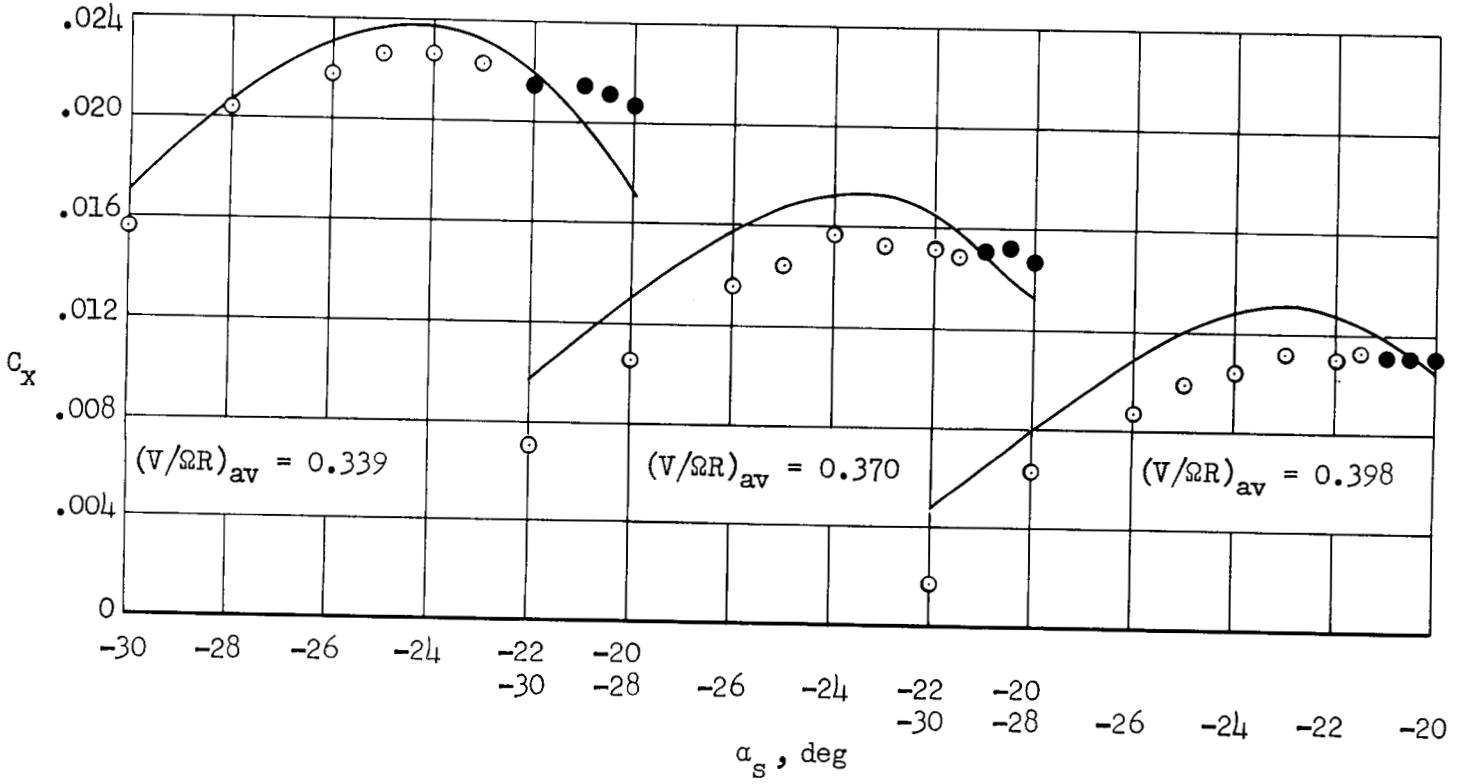

(b) $\theta_{0.75} = 15^\circ$

Figure 8.- Concluded.

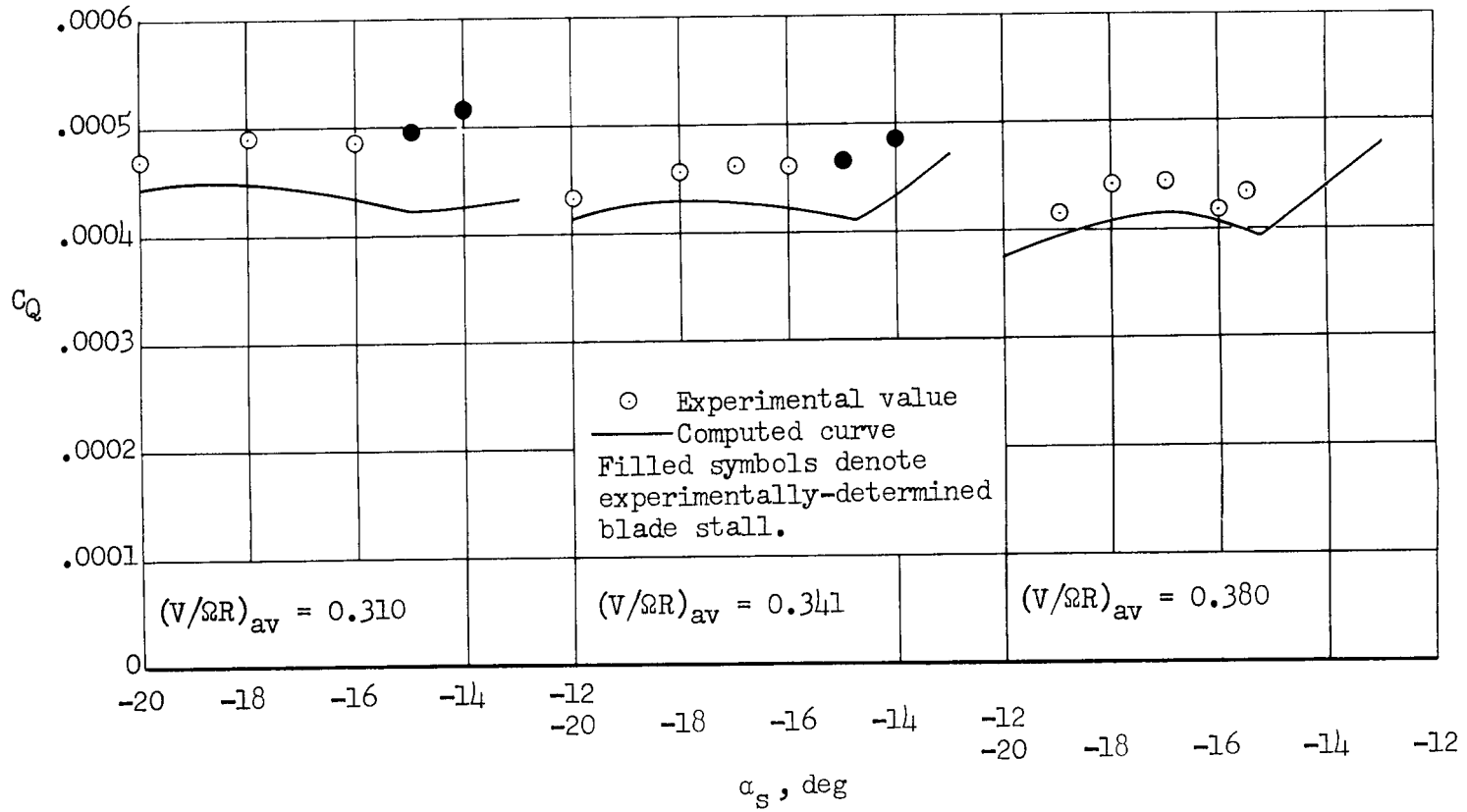

(a) $\theta_{0.75} = 12^\circ$

Figure 9.- Comparison of computed and experimental variations of C_Q with α_s.

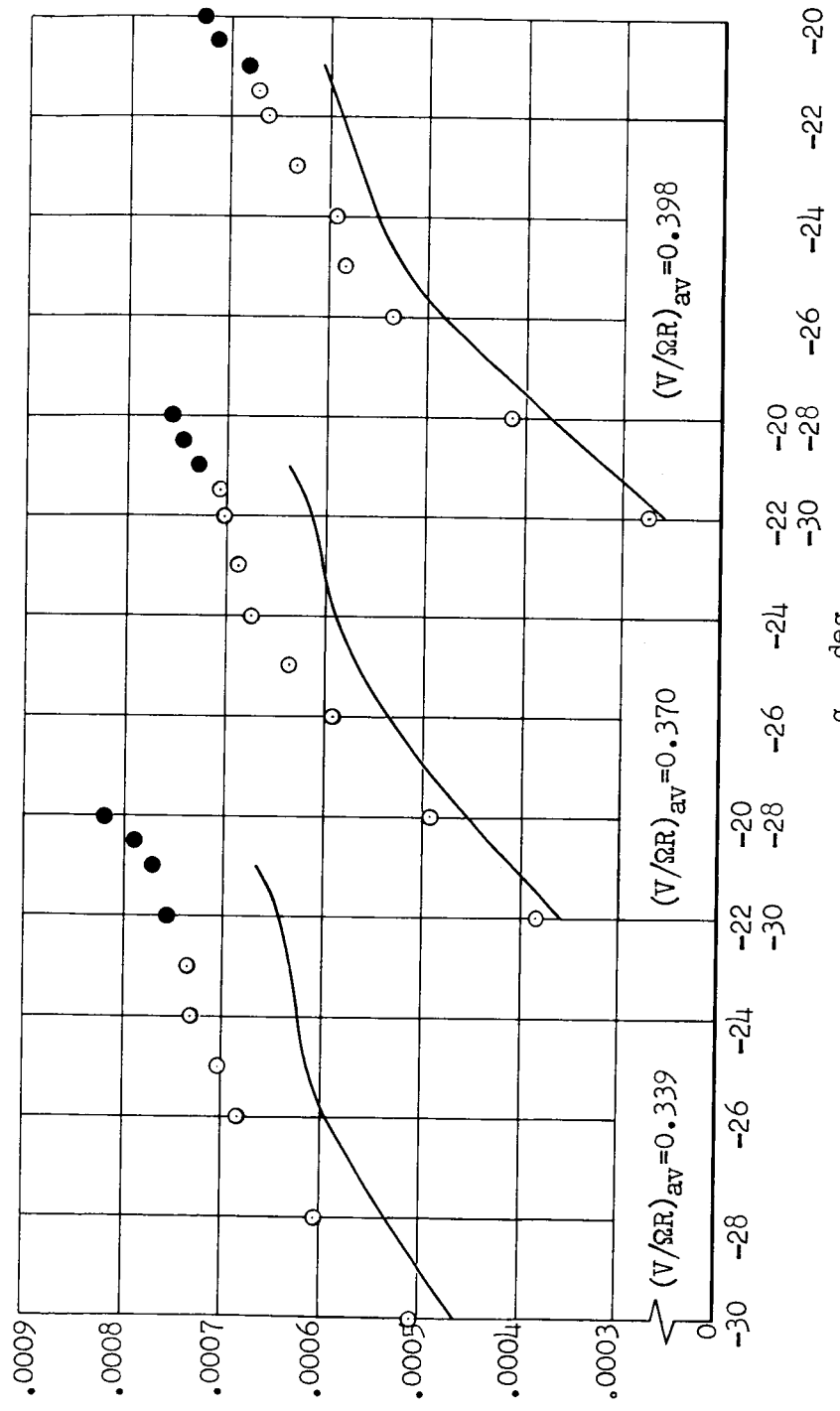

(b) $\theta_{0.75} = 15^\circ$

Figure 9.- Concluded.

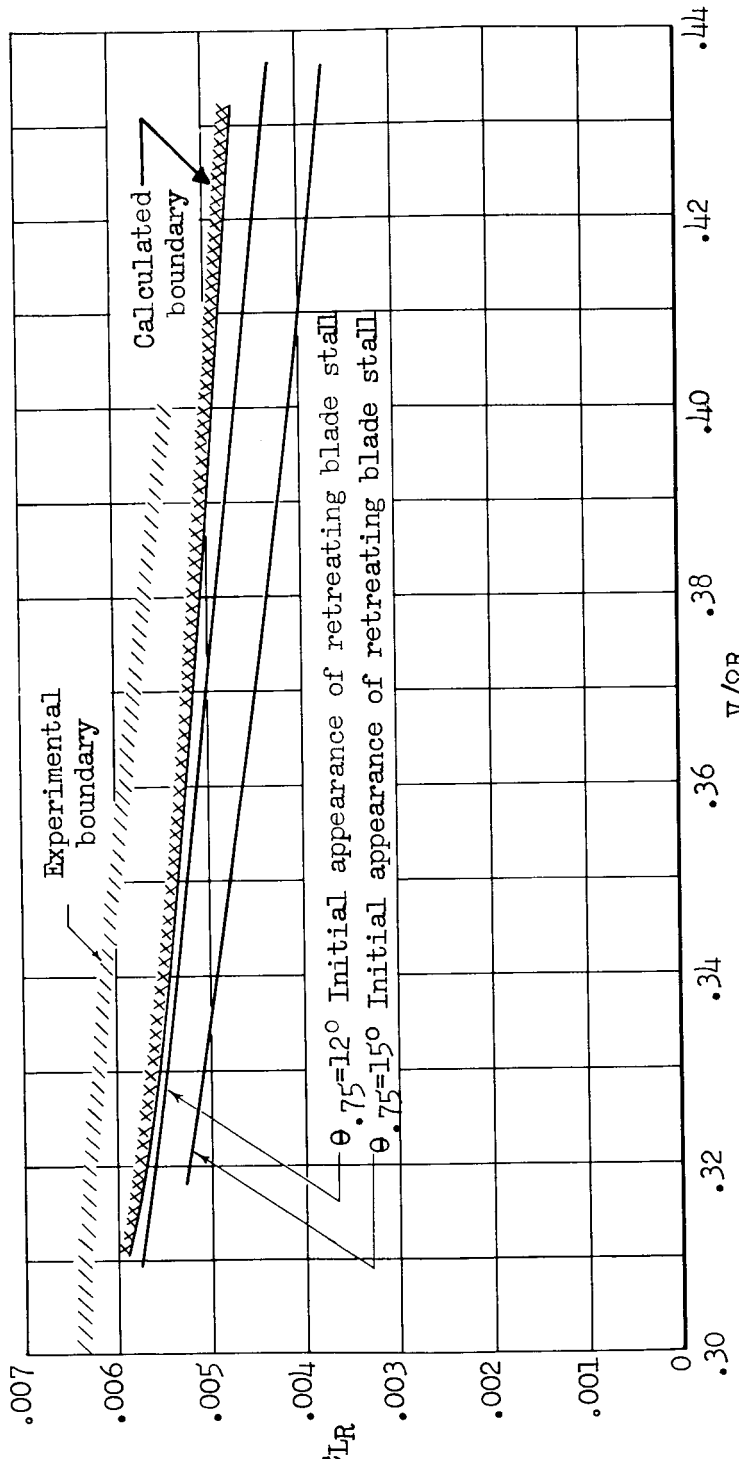

Figure 10.- Comparison of computed and experimental stall boundaries.